NANO LETTERS

Letter

pubs.acs.org/NanoLett

Direct Work Function Measurement by Gas Phase Photoelectron Spectroscopy and Its Application on PbS Nanoparticles

Stephanus Axnanda,[†,#] Marcus Scheele,[‡,#] Ethan Crumlin,[†] Baohua Mao,[†,∥] Rui Chang,[†,⊥] Sana Rani,[†] Mohamed Faiz,[§] Suidong Wang,[∥] A. Paul Alivisatos,[‡] and Zhi Liu*[,†]

[†]Advanced Light Source Division and [‡]Material Science Division, Lawrence Berkeley National Laboratory, Berkeley, California 94720

[§]Physics Department and CENT, King Fahd University of Petroleum and Minerals, Dhahran 31261, Saudi Arabia

[∥]Institute of Functional Nano and Soft Materials (FUNSOM), Soochow University, Suzhou, Jiangsu 215123, China

[⊥]State Key Laboratory of Functional Materials for Informatics, Shanghai Institute of Microsystem and Information Technology, Chinese Academy of Sciences, Shanghai 200050, China

S *Supporting Information*

ABSTRACT: Work function is a fundamental property of a material's surface. It is playing an ever more important role in engineering new energy materials and efficient energy devices, especially in the field of photovoltaic devices, catalysis, semiconductor heterojunctions, nanotechnology, and electrochemistry. Using ambient pressure X-ray photoelectron spectroscopy (APXPS), we have measured the binding energies of core level photoelectrons of Ar gas in the vicinity of several reference materials with known work functions (Au(111), Pt(111), graphite) and PbS nanoparticles. We demonstrate an unambiguously negative correlation between the work functions of reference samples and the binding energies of Ar 2p core level photoelectrons detected from the Ar gas near the sample surface region. Using this experimentally determined linear relationship between the surface work function and Ar gas core level photoelectron binding energy, we can measure the surface work function of different materials under different gas environments. To demonstrate the potential applications of this ambient pressure XPS technique in nanotechnology and solar energy research, we investigate the work functions of PbS nanoparticles with various capping ligands: methoxide, mercaptopropionic acid, and ethanedithiol. Significant Fermi level position changes are observed for PbS nanoparticles when the nanoparticle size and capping ligands are varied. The corresponding changes in the valence band maximum illustrate that an efficient quantum dot solar cell design has to take into account the electrochemical effect of the capping ligand as well.

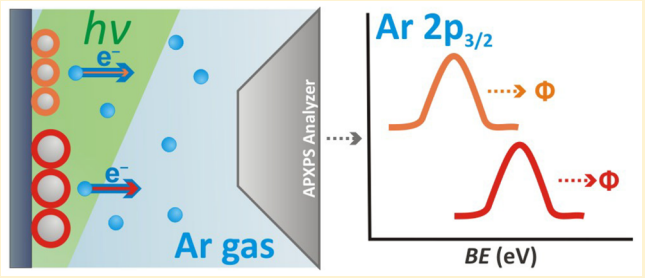

KEYWORDS: *Ambient pressure photoelectron spectroscopy, work function, nanoparticle, nanocrystal, photovoltaics, PbS*

Work function, the minimum energy needed to remove an electron from a solid to vacuum, is a key property of any material surface. It plays a crucial role in engineering new energy materials and devices, particularly in applications like photovoltaic/solar cells,[1−4] catalysis,[5−7] semiconductor devices,[8−11] and electrochemical devices.[1,12] Because of its surface sensitive nature, however, it remains a challenge to accurately measure the work function (WF). The value of WF depends on the surface cleanliness, reconstruction, adsorbates as well as the material's bulk electronic structure.[13]

Kelvin probe (KP)[5,14−17] and photoemission spectroscopy (PES)[18−23] are two widely used work function measurement techniques. Yet, both techniques have their limitations. For the KP method, the potential changes of the work function of the reference electrode surface due to surface contamination can affect its accuracy. In PES, the work function can in theory be readily determined by the difference between the low energy cutoff of the secondary electron tail and the valence band maximum. In practice, it is not trivial to define the low energy cutoff onset as well as the valence band maximum, particularly for semiconductors. Detailed knowledge of the density of state of the sample's valence band and photoelectron cross-section is needed to accurately determine the valence band maximum in the PES spectrum. This information is not always easily available for novel materials. Furthermore, PES and other work function methods, such as the field emission and the photoemission of adsorbed xenon (PAX) method, require ultra high vacuum conditions.[24,25]

Recent in situ studies have demonstrated that the gas environment can have profound impacts on the surface reconstruction of some materials.[26−28] To this end, the capability to measure a material's work function accurately under a wide range of conditions where the material will be used is highly advantageous. A technique that provides this

Received: September 20, 2013
Revised: October 28, 2013
Published: October 31, 2013

   dx.doi.org/10.1021/nl403524a | *Nano Lett.* 2013, 13, 6176−6182

advantage is gas phase core level X-ray photoelectron spectroscopy at ambient pressure.[29,30] Briefly speaking, core level spectroscopy of the same gas molecules used as a probe is performed in the vicinity of two different materials' surfaces. The detected change of the gas molecules' core level binding energy (BE) is a measure for the difference in work function between the two materials.[31,32]

In this study, using an APXPS apparatus, we are able to detect Ar 2p gas phase core level energy shifts in response to work function changes. By conducting measurements on well-known work function reference samples such as Au(111), Pt(111), and graphite, we validate the proposed linear relationship between the surface work function and Ar gas phase core level BE.[31−33] This linear relationship can be used directly to determine the work function of an unknown material's surface.

In the second part of this study, we apply this work function measurement technique to PbS nanoparticles with two different sizes (2.9 and 9.8 nm) and different capping ligands (methoxide, mercaptopropionic acid, and ethanedithiol) under controlled Ar environment. We observe a significant influence of the quantum confinement effect and the nature of the capping ligands onto the band positions. Upon correlation with carrier concentration measurements, we can determine the position of the top of the valence band maximum (VBM) in each nanoparticle sample. The results have immediate implications for the rational design of PbS-based quantum dot solar cells.

Experiments. APXPS experiments are performed at Beamline 9.3.2 of the Advanced Light Source. The apparatus consists of two connected vacuum chambers: one for sample preparation and one for analysis.[34,35] Pt(111), Au(111), and highly ordered pyrolytic graphite (HOPG) are used as reference samples. Both Pt(111) and Au (111) are purchased from Matek company. The ZYA grade HOPG is obtained commercially from Structure Probe Inc. Standard multicycles of sputter-and-anneal cleaning methods are used on the Pt(111) and Au(111) crystals. We sputter the samples in Ar gas at 1×10^{-5} Torr at 1 keV. The Pt(111) and Au(111) samples are annealed at 1000 and 850 K, respectively. A clean HOPG surface is prepared by cleaving with tape. The cleanliness of Pt(111) and Au(111) sample surfaces is verified by XPS. Photoelectron spectra of the core levels of interest are recorded at photon energies of 750 and 490 eV, respectively. In this experiment, we use CO (Air Gas, UHP), O_2 (Air Gas, UHP), and Ar (Air Gas, research grade) gases. Each of them is connected to the analysis chamber via individual UHV leak valves. A calibrated Baratron gauge is used to monitor the total pressures inside the analysis chamber.

Detailed descriptions of the PbS nanoparticle synthesis and sample preparation may be found in the Supporting Information. The nanoparticle samples are transferred into the APXPS chamber under inert conditions to prevent oxidation and modification of the nanoparticles' surface.

Results and Discussion. We use gas phase core level photoelectron spectroscopy to measure the surface work function. This concept is first described by Siegbahn and et al.[31,32] The principle of this technique is illustrated in Figure 1. In a photoelectron spectroscopy experiment, electrons are excited from different core levels and emitted (metal sample in Figure 1) as a consequence of photo excitation by X-ray photons ($h\nu$). The kinetic energies (KE_{samp}) of these photoelectrons can be measured through an electron energy

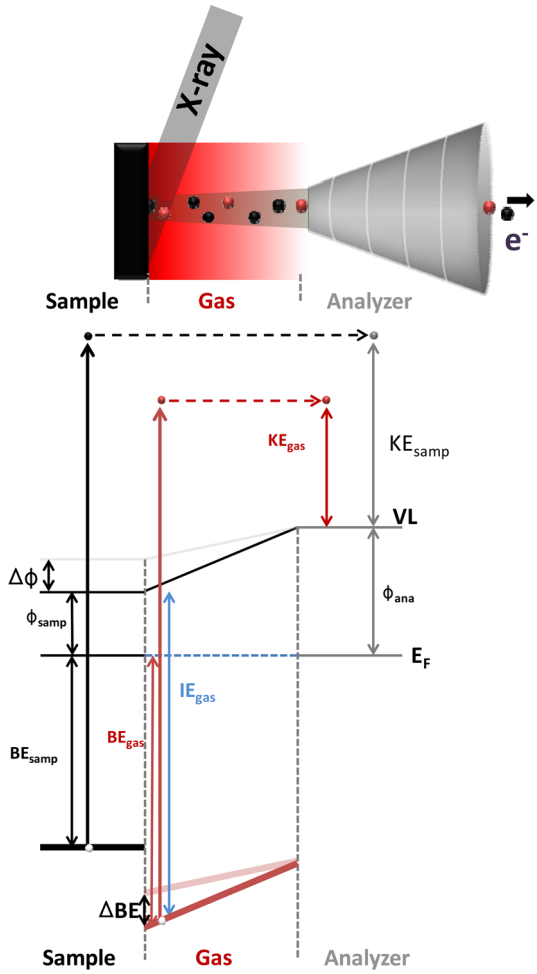

Figure 1. The schematic drawing of the energetics of core level photoelectron spectroscopy form a solid sample and gas molecules. The work function change, a relative change between the vacuum level at sample surface and the Fermi level, can be detected by measuring the BE changes of gas phase core level photoelectrons.

analyzer (Φ_{ana}). Therefore, we can obtain the binding energy of the core level of interest using the Einstein photoelectrical equation

$$BE_{samp} = h\nu - KE_{samp} - \Phi_{ana} \quad (1)$$

As the binding energy of a metal (BE_{samp}) is referenced to the Fermi level of the sample, BE_{samp} will not change as the work function of the sample (Φ_{samp}) changes. On the contrary, the ionization energy of the gas phase molecule (IE_{gas}) is referenced to the vacuum level. From eq 1 and $IE_{gas} = BE_{gas} + \Phi_{samp}$, the detected kinetic energy of a gas phase photoelectron from the near surface region is

$$KE_{gas} = h\nu - BE_{gas} - \Phi_{ana} = h\nu - IE_{gas} + \Phi_{samp} - \Phi_{ana} \quad (2)$$

As shown in Figure 1, the vacuum level of gas molecules in the vicinity of a solid sample's surface is determined by the material surface work function. Since IE_{gas} is constant for a given free gas molecule, the change of the vacuum level relative to the Fermi level must induce a corresponding change in the detected binding energy of the gas phase core level photoelectrons. This detected binding energy change (ΔBE_{gas}) of the gas phase can be used to monitor the work function change

dx.doi.org/10.1021/nl403524a | Nano Lett. 2013, 13, 6176−6182

($\Delta\Phi_{samp}$) between different samples. If these samples have known and well-studied work functions, BE_{gas} can be translated into Φ_{samp}.

Depending on where the gas phase photoelectron is created, its binding energy change ΔBE_{gas} will change by a lesser amount for a given work function change $\Delta\Phi_{samp}$ at the surface. Only for a photoelectron emitted from the very near surface region, $\Delta BE_{gas} = -\Delta\Phi_{samp}$. The further the photoelectron is created away from the surface, the less the binding energy change ΔBE_{gas} is. Therefore, the change of BE_{gas} is also position dependent, which may be accounted for by introducing a geometry correction factor (c), such that $\Delta BE_{gas} = -c\Delta\Phi_{samp}$. This correction factor reflects the average position from where the photoelectrons of gas molecules are emitted. It depends on the width of the X-ray beam, its incident angle to the surface, and the distance between sample and the first aperture (how the gas molecules are illuminated). It is a system and experiment dependent correction factor. Once this factor is determined for a given system, the absolute work function of a given sample can be determined through gas phase core level peak shift.

$$BE_{gas} = -c\Phi_{samp} + b \quad (3)$$

where b is a constant.

Although this technique has been proposed decades ago,[32] there is no previous experimental validation study of eq 3. Because of the cone shape geometry of the analyzer opening and other nonideal environments in a realistic APXPS system, it is unclear if we can use such a method to measure the absolute work function of a given surface. Therefore, it is important to study well-known samples first to validate and establish this technique. In this study, we directly compare three well-studied work function reference samples to the measurements of the Ar 2p BE from Ar gas phase. The samples are highly ordered pyrolytic graphite (HOPG), Au(111), and Pt(111). From literature, the reported work function values of these reference samples are 4.4−4.8 eV for HOPG;[36−39] 5.15−5.38 eV for Au(111);[40−45] 5.7−6.1 eV for Pt(111).[46−52] When the BEs of Ar 2p photoelectrons emitted from the near surface region of these reference samples are plotted against the reported work function values, a linear dependence is expected if the eq 3 above holds. By fitting the measured BE_{gas} values, we can obtain the geometry correction factor c and the constant b for our APXPS endstation.

Figure 2 shows Ar 2p spectra of Ar gas in the near surface region of HOPG, Au(111), and Pt(111). As shown in Figure 2, the Ar 2p BEs are different for different sample surfaces. By fitting the spectrum using a Gaussian line shape, the BE_{gas} of Ar $2p_{3/2}$ peak can be determined. The BE_{gas} of Ar $2p_{3/2}$ measured from the near surface region of HOPG, Au(111), and Pt(111) are 244.2, 243.5, and 243.1 eV, respectively. We can see that the Ar 2p core level BE is smaller for the sample with higher work function as predicted by eq 3. We plot reported work function values versus Ar $2p_{3/2}$ BE in Figure 3. We find a clearly negative correlation between the Φ_{samp} and BE_{gas}. From eq 3, the work function of the sample is

$$\Phi_{samp} = -\frac{BE_{gas}}{c} + \frac{b}{c}$$

The linear regression fit of reference samples data shown in Figure 3 gives the following equation

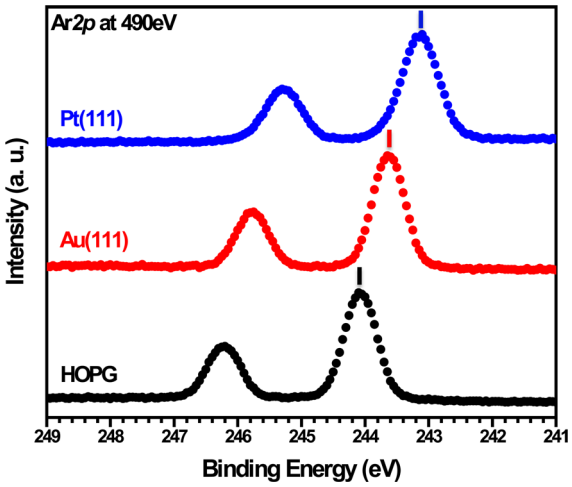

Figure 2. Ar 2p XPS spectra of 250 mTorr Ar gas phase at the near surface region of (black) graphite, (red) Au(111), and (blue) Pt(111). Photon energy is 490 eV.

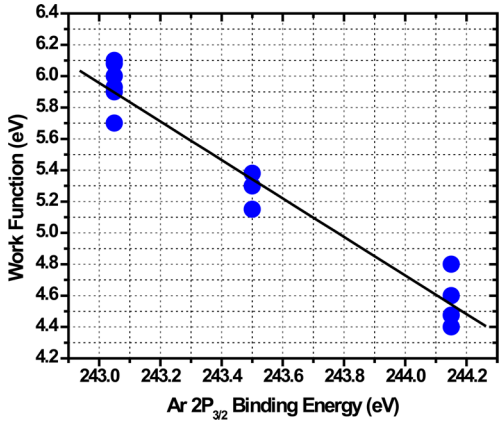

Figure 3. Work function versus measured Ar $2p_{3/2}$ gas phase binding energy values. The work function values are of HOPG, Au(111), and Pt(111) from listed references. The Ar $2p_{3/2}$ BEs are measured from near surface of HOPG, Au(111), and Pt(111) at 250 mTorr of Ar gas for each measurement.

$$\Phi_{samp} = -1.228BE_{gas} + 304.46 \quad (4)$$

where the coefficient of determination R^2 is 0.94. The geometry correction factor c is 0.81, indicating that a substantial fraction of molecules were captured some distance away from the solid sample's surface which decreases the change in their vacuum level.

Comparing the Ar $2p_{3/2}$ BEs detected from different reference samples, we have demonstrated that the Ar gas phase core level binding energies measured in the vicinity of different materials' surfaces indeed depend linearly on their work functions. Thus, eq 3 holds in our APXPS experiments. The complex geometry of the cone opening of a real APXPS system has only minimum impact on the work function measurement. We can now use eq 4 to convert the measured Ar 2p BE value into the work function value of unknown materials' surfaces.

In addition to inert gases like Ar, other gases such as CO, O_2, and gas mixtures can also be used to measure work function. Precaution must be taken for each system when reactive gases are used. In the Supporting Information, we present how CO and O_2 can be used to determine the work function. An

dx.doi.org/10.1021/nl403524a | Nano Lett. 2013, 13, 6176−6182

Table 1. Length, Nanoparticle Diameter, Excitonic Transition Energy, Effective Density of States, Carrier Concentrations and $E_F - E_H$ Values for PbS Nanoparticles Stabilized with Different Ligands[a]

ligand	length/Å	diameter/nm	$1S_e \leftarrow 1S_h$ / eV	N_H (QDS, 9.8 nm)/cm^{-3}	n_h/cm^{-3}	$E_F - E_H$/ eV
MeO^-	3	2.9	1.56	2.3×10^{20}	immeasurable*	0.23
MeO^-	3	9.8	0.59	7.4×10^{18}	2.5×10^{16}	0.15
EDT	5	9.8	0.59	7.0×10^{18}	3.3×10^{15}	0.20
MPA	5	9.8	0.59	7.0×10^{18}	2×10^{16}	0.15

[a][*] The carrier concentration for this sample was estimated by assuming a size-invariant behavior as explained in the text.

alternative calibration procedure is also described. We can bias the sample to obtain the geometric correcting factor without using multiple reference samples.

The ability to use reactant gases to track work function changes is particularly important. On the one hand, we can now probe and follow the change of work function under realistic conditions during the reaction. An example of a CO oxidation experiment on a model catalyst Pd(100) surface is given in the Supporting Information.[53]

On the other hand, detailed structural information, such as the adsorption sites of gas molecules at the gas−solid interface, can be extracted through the work function measurement. The gas adsorbates such as CO and NO will induce work function changes on transition metal (TM) surfaces due to the electron donation and back-donation from the adsorbate to the metal surface. Such processes are carried out through the interplay between adsorbate molecular orbital and TM *d*-bands. The extents of the electron transfer depend critically on the coordination number (adsorption sites) and TM *d*-band filling.[54] Thus, the work function changes on these surfaces are very sensitive to the adsorption sites. With the help of gas phase core level information, we can not only determine the chemical states of adsorbates and underlying surface but also provide additional structural information of adsorption sites at different coverages.

Work Function Measurements of Semiconductor Nanoparticle Samples. To demonstrate the potential applications of this ambient pressure XPS technique in nanotechnology and solar energy research, PbS nanoparticles with different size and different capping ligands are investigated to study the effects toward their work functions.

Semiconductor nanoparticles, or quantum dots, are important materials due to their large potential for applications in nanotechnology, optoelectronics and biology.[55,56] For example, PbS is a material that is widely used in diodes, infrared detectors, optic fibers, window coatings, and solar energy panels.[57,58] The optical and electronic properties of semiconductor nanoparticles can be tuned by the quantum size effect and the dielectric environment.[58,59] Many efforts have focused on controlling the properties of PbS nanoparticles by controlling the size and also adding different ligands to the system to modify its energy gap.

It is difficult to accurately determine the work function of semiconducting colloidal nanoparticle (NP) system because of its complexity. The $1S_h$ states of various NPs like CdSe, CdTe, PbS, and PbSe have been found to be dependent on the nature of the capping ligand binding to the NPs' surface and the substrate on which the sample was deposited.[60−63] Using photoemission spectroscopy in ultrahigh vacuum, the valence band maximum of CdS nanoparticles has been shown to be strongly dependent on the NP diameter which was interpreted as a signature of the quantum confinement effect.[64] Recently, colloidal nanoparticles, in particular PbS, have been successfully applied as light absorbers in solar cell devices with efficiencies of up to 7%.[4] The complex architecture of these nanoparticle devices with several solid state interfaces, different NP sizes, and a variety of applied surface treatments requires a more precise determination of the materials' work functions under actual testing conditions, that is, in an ambient environment.

We study two PbS nanoparticle samples by APXPS and the effect of ligand exchange with the capping molecules methoxide (MeO^-), mercaptopropionic acid (MPA), and ethanedithiol (EDT). These ligands in combination with PbS quantum dots are commonly applied as the absorbing layer in state-of-the-art quantum dot solar cells. The first sample consists of particles of 2.9 nm (±20%) diameter with a $1S_e \leftarrow 1S_h$ transition energy of 1.56 eV, where the second sample shows 9.8 nm (±18%) diameter and a 0.59 eV energy level gap. For further details to synthesis and characterization of theses nanoparticles and the ligand exchange, the reader is referred to the Supporting Information (Figures S1 and S2).

In a nondegenerate semiconductor, the difference between the Fermi level (E_F) and the highest occupied hole state (E_H; $1S_h$ in a quantum dot, the VBM in a bulk material) is given by

$$E_F - E_H = kT \ln\left(\frac{N_H}{n_h}\right)$$

with the Boltzmann constant (k), the absolute temperature (T), the concentration of free holes (n_h), and the effective density of states near the highest occupied hole state (N_H). In a quantum dot solid (QDS), N_H is approximately given by applying an effective medium approach according to

$$N_{H,QDS} = 2M_H \, FF \, V^{-1}$$

with the fill factor (FF), that is, the volume fraction occupied by quantum dots, the degeneracy of the valence band maximum (M_H), and the volume of an individual quantum dot (V). We use $M_H = 4$, $FF = 0.5$, and assume a spherical particle shape to estimate V. For the effective diameter, we add the bare nanoparticle diameter derived from electron microscopy to the nominal length of each ligand studied to account for the additional volume occupied by the ligand sphere. We derive the hole concentration by measuring a thin film of the same nanoparticles in a field effect transistor geometry.[65,66] Where details to this measurement can be found in the Supporting Information, Table 1 summarizes the measured hole concentrations and corresponding values for $E_F - E_H$ for 2.9 and 9.8 nm PbS nanoparticles stabilized with MeO^-, EDT and MPA as well as the nominal ligands' length and the calculated effective density of states.

No operational field-effect transistors could be fabricated from 2.9 nm PbS particles consistent with the finding that QDS from small nanoparticles are often poorly conducting due to the large charging energies associated with carrier injection. Hence, we can only speculate about $E_F - E_H$ in this sample. In a recent

dx.doi.org/10.1021/nl403524a | Nano Lett. 2013, 13, 6176−6182

study of lead chalcogenide nanoparticles capped with the methoxide ion, no significant changes in the carrier concentration was found upon varying the nanoparticle diameter between 3.0 and 8.9 nm.[67] We therefore assume the carrier concentrations of the two PbS particle samples capped with MeO^- used in this work to be of similar magnitude.

In Figure 4, the Ar binding energies in the near surface region of the four PbS samples studied here are shown. We

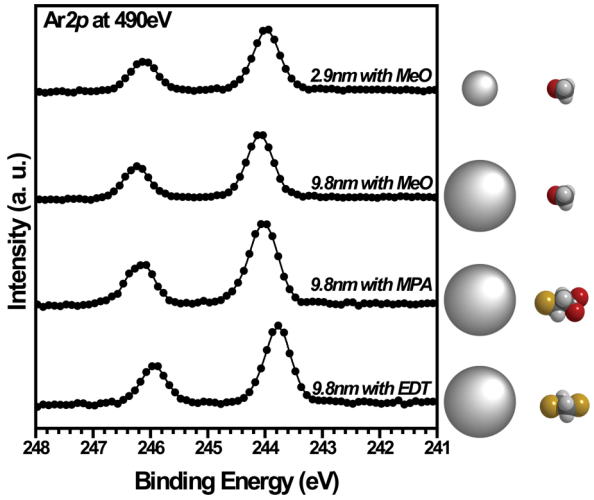

Figure 4. Ar 2p spectra from near surface region of PbS nanoparticle samples with different ligands: 2.9 nm PbS with MeO^- ligand, 9.8 nm PbS with methoxide ligand, 9.8 nm PbS with mercaptopropionic acid ligand, and 9.8 nm PbS with ethanedithiol ligand. The pressure of Ar gas is 250 mTorr. The spectra are taken at 490 eV photon energy.

convert the binding energies into the corresponding work functions by using eq 4 and compare the effect of nanoparticle size for MeO^- capped PbS nanoparticles as well as the effect of varying surface ligands onto 9.8 nm PbS particles in Figure 5.

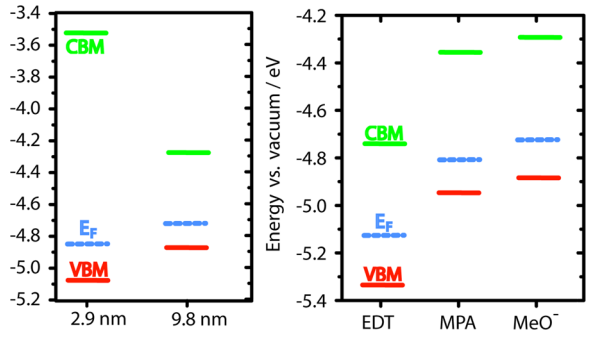

Figure 5. Fermi level, VBM, and CBM values of PbS nanoparticles with different diameter and methoxide capping (left) as well as different ligands and 9.8 nm diameter (right). Dashed lines show the measured Fermi level and full lines indicate the calculated VBM (red) and CBM (green).

On using the values for E_F-E_H in Table 1 and the excitonic transition energies from absorption spectroscopy, we also plot the corresponding values for the VBM and conduction band minimum (CBM) of each sample.

Increasing the bandgap in MeO^- capped PbS nanoparticles from 0.59 to 1.56 eV causes a depression of the Fermi level by 0.14 eV from −4.72 to −4.86 eV against vacuum. This is consistent with the findings that (a) the VBM descends in energy due to an increase in confinement energy and (b) the Fermi level only partially follows the VBM since E_F-E_H widens due to the increased effective density of states in quantum dot solids with a smaller nanoparticle diameter.[64]

More importantly, we note significant energy differences not only for the Fermi level but also for the band edges for PbS nanoparticles of the same size but with different classes of surface ligands. Capping with MeO^- or MPA (−4.95 eV) leads to a significantly higher VBM position than capping with EDT (−5.33 eV). Similar results have been reported for CdSe and InAs nanoparticles with VBM shifts of as much as 0.4 eV depending on the ligand.[60,61,63] In the case of CdSe, it was suggested that these differences may be explained by the degree of hole scavenging and surface passivation. A ligand with suitable trap sites for holes or poor binding affinity and incomplete surface site passivation (thiols, pyridine) was found to induce a lower VBM position than ligands without these properties (primary amines in the case of CdSe). When comparing our VBM measurement results for EDT versus MPA capping, this explanation is seen to hold true also for p-type PbS nanoparticles. Jeong et al. have measured longer transient absorption lifetimes for EDT capping (93 μs) than for MPA stabilization (31 μs) indicative of a smaller trap state density in the latter case.[68] Tang et al. showed that EDT induces deeper intraband trap states than MPA capping of PbS nanoparticles.[69] Within the picture of hole scavenging and incomplete surface passivation, both of these results may be reflected in the 0.38 eV lower VBM of EDT-capped PbS nanoparticles displayed in Figure 5.

Finally, we find that capping with MeO^- also leads to a shallow work function similar to MPA capping. No comparative information on the density or depth of trap states is available for this treatment. In combination with annealing in air, it has been demonstrated to result in degenerate p-doping in PbS nanoparticles such that one could expect a relatively large trap state density. Without this annealing step, we measure p-type behavior and a hole density of 2.5×10^{16} cm^{-3} which is comparable to ligand exchange with MPA (see Supporting Information for details). This implies that MeO^- could be an alternative to MPA capping to result in p-type absorbing layers for efficient quantum dot photovoltaic devices.

Conclusions. Using gas phase core level photoelectron spectroscopy, we measure the work function of PbS nanoparticles as a function of size and type of capping ligand. By observing the change in core level binding energy of argon gas in the vicinity of highly ordered pyrolytic graphite, Au(111) and Pt(111), we correlate each measured change with the reported work function of each individual surface and obtain a calibration curve that accounts for geometrical factors of the measurement setup. Using this calibration, we measure the work function of a variety of PbS nanoparticle samples functionalized with different surface ligands under a pressure of 250 mTorr Ar gas and, thus, near-working conditions for optoelectronic devices. Upon correlation with carrier concentrations extracted from field-effect transistor measurements, we also calculate the position of the top of the valence band (VBM) in each nanoparticle sample. Our results highlight the great sensitivity of the VBM onto the type of capping ligand that may be interpreted with varying degrees of surface passivation.

Gas phase core level photoelectron spectroscopy can overcome the limitations of some traditional work function measurement methods such as the requirements of ultrahigh

dx.doi.org/10.1021/nl403524a | Nano Lett. 2013, 13, 6176−6182

vacuum condition. With this method, the materials' work functions can be measured at various controlled pressures and temperatures, including near-ambient conditions. We believe the successful and continuing development of this APXPS technique will have important impacts on many important fields such as photovoltaics, light-emitting diodes, and catalysis.

■ ASSOCIATED CONTENT

Supporting Information

(1) PbS nanoparticles synthesis and sample preparation. (2) Work function measurement using CO and oxygen. (3) The work function change during the CO oxidation on Pd(100) surface. This material is available free of charge via the Internet at http://pubs.acs.org.

■ AUTHOR INFORMATION

Corresponding Author

*E-mail: zliu2@lbl.gov.

Author Contributions

The manuscript was written through contributions of all authors. All authors have given approval to the final version of the manuscript.

Author Contributions

#S.A. and M.S. contributed equally.

Notes

The authors declare no competing financial interest.

■ ACKNOWLEDGMENTS

Nanoparticle synthesis and characterization, ligand exchange, sample preparation and transport measurements were funded by the Self-Assembly of Organic/Inorganic Nanocomposite Materials program (Grant DE-AC02-05CH11231 to A.P.A) which is supported by the Director, Office of Science, Office of Basic Energy Sciences of the U.S. Department of Energy under Contract No. DE-AC02-05CH11231. The Advanced Light Source is supported by the Director, Office of Science, Office of Basic Energy Sciences, of the U.S. Department of Energy under Contract No. DE-AC02-05CH11231. M.S. would like to thank the Alexander von Humboldt-Foundation for a Feodor Lynen-Fellowship. R.C. is supported by National Natural Science Foundation of China under contract No. 11227902. We are grateful to Jesse Engel for inspiring discussions and advice on applying the effective medium approach.

■ REFERENCES

(1) Gratzel, M. *Nature* **2001**, *414* (6861), 338−344.
(2) Scharber, M. C.; Mühlbacher, D.; Koppe, M.; Denk, P.; Waldauf, C.; Heeger, A. J.; Brabec, C. J. *Adv. Mater.* **2006**, *18* (6), 789−794.
(3) Tang, J.; Brzozowski, L.; Barkhouse, D. A. R.; Wang, X.; Debnath, R.; Wolowiec, R.; Palmiano, E.; Levina, L.; Pattantyus-Abraham, A. G.; Jamakosmanovic, D.; Sargent, E. H. *ACS Nano* **2010**, *4* (2), 869−878.
(4) Ip, A. H.; Thon, S. M.; Hoogland, S.; Voznyy, O.; Zhitomirsky, D.; Debnath, R.; Levina, L.; Rollny, L. R.; Carey, G. H.; Fischer, A.; Kemp, K. W.; Kramer, I. J.; Ning, Z.; Labelle, A. J.; Chou, K. W.; Amassian, A.; Sargent, E. H. *Nat. Nanotechnol.* **2012**, *7* (9), 577−582.
(5) Heiland, G. *Ber. Bunsen-Ges. Phys. Chem.* **1975**, *79* (7), 641−641.
(6) Wittstock, A.; Zielasek, V.; Biener, J.; Friend, C. M.; Bäumer, M. *Science* **2010**, *327* (5963), 319−322.
(7) Berr, M. J.; Schweinberger, F. F.; Döblinger, M.; Sanwald, K. E.; Wolff, C.; Breimeier, J.; Crampton, A. S.; Ridge, C. J.; Tschurl, M.; Heiz, U.; Jäckel, F.; Feldmann, J. *Nano Lett.* **2012**, *12* (11), 5903−5906.
(8) Brillson, L. J. *Surf. Sci. Rep.* **1982**, *2* (2), 123−326.
(9) Chung, D. S.; Lee, J.-S.; Huang, J.; Nag, A.; Ithurria, S.; Talapin, D. V. *Nano Lett.* **2012**, *12* (4), 1813−1820.
(10) Kim, D. K.; Lai, Y.; Diroll, B. T.; Murray, C. B.; Kagan, C. R. *Nat. Commun.* **2012**, *3*, 1216.
(11) Liu, Y.; Tolentino, J.; Gibbs, M.; Ihly, R.; Perkins, C. L.; Liu, Y.; Crawford, N.; Hemminger, J. C.; Law, M. *Nano Lett.* **2013**, *13* (4), 1578−1587.
(12) Bard, A. J.; Faulkner, L. R. *Electrochemical Methods: Fundamentals and Applications*; Wiley: New York: 1980; Vol. *2*.
(13) Braun, S.; Salaneck, W. R.; Fahlman, M. *Adv. Mater.* **2009**, *21* (14−15), 1450−1472.
(14) Zisman, W. A. *Rev. Sci. Instrum.* **1932**, *3* (7), 367−370.
(15) Besocke, K.; Berger, S. *Rev. Sci. Instrum.* **1976**, *47* (7), 840−842.
(16) Saito, S.; Soumura, T.; Maeda, T. *J. Vac. Sci. Technol., A* **1984**, *2* (3), 1389−1391.
(17) Baikie, I. D.; Venderbosch, E.; Meyer, J. A.; Estrup, P. J. Z. *Rev. Sci. Instrum.* **1991**, *62* (3), 725−735.
(18) Berglund, C. N.; Spicer, W. E. *Phys. Rev.* **1964**, *136* (4A), A1030−A1044.
(19) Hüfner, S. *Photoelectron spectroscopy: principles and applications*; Springer-Verlag: New York, 1995.
(20) Ley, L.; Cardona, M. *Photoemission in Solids I*; Springer Berline Heidelberg: Berlin, 1978; Vol. *26*.
(21) Sun, Y.; Liu, Z.; Pianetta, P. *J Vac. Sci. Technol., A* **2007**, *25* (5), 1351−1356.
(22) LaRue, J. L.; White, J. D.; Nahler, N. H.; Liu, Z.; Sun, Y.; Pianetta, P. A.; Auerbach, D. J.; Wodtke, A. M. *J. Chem. Phys.* **2008**, *129* (2), 024709.
(23) Allen, F. G.; Gobeli, G. W. *Phys. Rev.* **1966**, *144* (2), 558−575.
(24) Wandelt, K. *J. Vac. Sci. Technol., A* **1984**, *2* (2), 802−807.
(25) Wandelt, K. *Appl. Surf. Sci.* **1997**, *111* (0), 1−10.
(26) Tao, F.; Grass, M. E.; Zhang, Y. W.; Butcher, D. R.; Renzas, J. R.; Liu, Z.; Chung, J. Y.; Mun, B. S.; Salmeron, M.; Somorjai, G. A. *Science* **2008**, *322* (5903), 932−934.
(27) Tao, F.; Dag, S.; Wang, L. W.; Liu, Z.; Butcher, D. R.; Bluhm, H.; Salmeron, M.; Somorjai, G. A. *Science* **2010**, *327* (5967), 850−853.
(28) Butcher, D. R.; Grass, M. E.; Zeng, Z. H.; Aksoy, F.; Bluhm, H.; Li, W. X.; Mun, B. S.; Somorjai, G. A.; Liu, Z. *J. Am. Chem. Soc.* **2011**, *133* (50), 20319−20325.
(29) Salmeron, M.; Schlögl, R. *Surf. Sci. Rep.* **2008**, *63* (4), 169−199.
(30) Starr, D. E.; Liu, Z.; Havecker, M.; Knop-Gericke, A.; Bluhm, H. *Chem. Soc. Rev.* **2013**, *42* (13), 5833−5857.
(31) Siegbahn, H.; Lundholm, M. *J. Electron Spectrosc. Relat. Phenom.* **1982**, *28* (1), 135−138.
(32) Siegbahn, H. *J. Phys. Chem.* **1985**, *89* (6), 897−909.
(33) Crumlin, E. J.; Bluhm, H.; Liu, Z. *J. Electron Spectrosc. Relat. Phenom.* **2013**, DOI: 10.1016/j.elspec.2013.03.002.
(34) Grass, M. E.; Karlsson, P. G.; Aksoy, F.; Lundqvist, M.; Wannberg, B.; Mun, B. S.; Hussain, Z.; Liu, Z. *Review of Scientific Instruments* **2010**, *81* (5), 053106.
(35) Aksoy, F.; Grass, M. E.; Joo, S. H.; Jabeen, N.; Hong, Y. P.; Hussain, Z.; Mun, B. S.; Liu, Z. *Nuclear Instruments & Methods in Physics Research Section a-Accelerators Spectrometers Detectors and Associated Equipment* **2011**, *645* (1), 260−265.
(36) Ago, H.; Kugler, T.; Cacialli, F.; Salaneck, W. R.; Shaffer, M. S. P.; Windle, A. H.; Friend, R. H. *J. Phys. Chem. B* **1999**, *103* (38), 8116−8121.
(37) Suzuki, S.; Bower, C.; Watanabe, Y.; Zhou, O. *Appl. Phys. Lett.* **2000**, *76* (26), 4007−4009.
(38) Hansen, W. N.; Hansen, G. J. *Surf. Sci.* **2001**, *481* (1−3), 172−184.
(39) Shiraishi, M.; Ata, M. *Carbon* **2001**, *39* (12), 1913−1917.
(40) Pescia, D.; Meier, F. *Surf. Sci.* **1982**, *117* (1−3), 302−309.
(41) Lecoeur, J.; Bellier, J. P.; Koehler, C. *Electrochim. Acta* **1990**, *35* (9), 1383−1392.
(42) Tzeng, C. T.; Lo, W. S.; Yuh, J. Y.; Chu, R. Y.; Tsuei, K. D. *Phys. Rev. B* **2000**, *61* (3), 2263−2272.
(43) Hagen, S.; Leyssner, F.; Nandi, D.; Wolf, M.; Tegeder, P. *Chem. Phys. Lett.* **2007**, *444* (1−3), 85−90.

(44) Duhm, S.; Gerlach, A.; Salzmann, I.; Bröker, B.; Johnson, R. L.; Schreiber, F.; Koch, N. *Org. Electron.* **2008**, *9* (1), 111−118.
(45) Otálvaro, D.; Veening, T.; Brocks, G. *J. Phys. Chem. C* **2012**, *116* (14), 7826−7837.
(46) Nieuwenhuys, B. E.; Sachtler, W. M. H. *Surf. Sci.* **1973**, *34* (2), 317−336.
(47) Nieuwenhuys, B. E.; Meijer, D. T.; Sachtler, W. M. H. *Phys. Status Solidi, A* **1974**, *24* (1), 115−122.
(48) Nieuwenhuys, B. E. *Surf. Sci.* **1976**, *59* (2), 430−446.
(49) Collins, D. M.; Spicer, W. E. *Surf. Sci.* **1977**, *69* (1), 114−132.
(50) Fisher, G. B. *Chem. Phys. Lett.* **1981**, *79* (3), 452−458.
(51) Salmerón, M.; Ferrer, S.; Jazzar, M.; Somorjai, G. A. *Phys. Rev. B* **1983**, *28* (12), 6758−6765.
(52) Derry, G. N.; Ji-Zhong, Z. *Phys. Rev. B* **1989**, *39* (3), 1940−1941.
(53) Blomberg, S.; Hoffmann, M. J.; Gustafson, J.; Martin, N. M.; Fernandes, V. R.; Borg, A.; Liu, Z.; Chang, R.; Matera, S.; Reuter, K.; Lundgren, E. *Phys. Rev. Lett.* **2013**, *110*, 117601.
(54) Zeng, Z.-H.; Da Silva, J. L. F.; Li, W.-X. *Phys. Chem. Chem. Phys.* **2010**, *12* (10), 2459−2470.
(55) Huynh, W. U.; Dittmer, J. J.; Alivisatos, A. P. *Science* **2002**, *295* (5564), 2425−2427.
(56) Klimov, V. I.; Mikhailovsky, A. A.; Xu, S.; Malko, A.; Hollingsworth, J. A.; Leatherdale, C. A.; Eisler, H.-J.; Bawendi, M. G. *Science* **2000**, *290* (5490), 314−317.
(57) Lieber, C. M.; Wu, X. L. *Acc. Chem. Res.* **1991**, *24* (6), 170−177.
(58) Souici, A. H.; Keghouche, N.; Delaire, J. A.; Remita, H.; Etcheberry, A.; Mostafavi, M. *J. Phys. Chem. C* **2009**, *113* (19), 8050−8057.
(59) Peterson, J. J.; Krauss, T. D. *Nano Lett.* **2006**, *6* (3), 510−514.
(60) Jasieniak, J.; Califano, M.; Watkins, S. E. *ACS Nano* **2011**, *5* (7), 5888−5902.
(61) Soreni-Harari, M.; Yaacobi-Gross, N.; Steiner, D.; Aharoni, A.; Banin, U.; Millo, O.; Tessler, N. *Nano Lett.* **2008**, *8* (2), 678−684.
(62) Timp, B. A.; Zhu, X. Y. *Surf. Sci.* **2010**, *604* (17−18), 1335−1341.
(63) Munro, A. M.; Zacher, B.; Graham, A.; Armstrong, N. R. *ACS Appl. Mater. Interfaces* **2010**, *2* (3), 863−869.
(64) Colvin, V. L.; Alivisatos, A. P.; Tobin, J. G. *Phys. Rev. Lett.* **1991**, *66* (21), 2786−2789.
(65) Dalven, R. *Infrared Phys.* **1969**, *9* (4), 141−184.
(66) Kang, I.; Wise, F. W. *J. Opt. Soc. Am. B* **1997**, *14* (7), 1632−1646.
(67) Scheele, M.; Engel, J. H.; Ferry, V. E.; Hanifi, D.; Liu, Y.; Alivisatos, A. P. *ACS Nano* **2013**, *7* (8), 6774−6781.
(68) Jeong, K. S.; Tang, J.; Liu, H.; Kim, J.; Schaefer, A. W.; Kemp, K.; Levina, L.; Wang, X.; Hoogland, S.; Debnath, R.; Brzozowski, L.; Sargent, E. H.; Asbury, J. B. *ACS Nano* **2011**, *6* (1), 89−99.
(69) Tang, J.; Kemp, K. W.; Hoogland, S.; Jeong, K. S.; Liu, H.; Levina, L.; Furukawa, M.; Wang, X.; Debnath, R.; Cha, D.; Chou, K. W.; Fischer, A.; Amassian, A.; Asbury, J. B.; Sargent, E. H. *Nat. Mater.* **2011**, *10* (10), 765−771.